Radiation-Driven Hydrodynamics of High-*Z* Hohlraums on the National Ignition Facility

E. L. Dewald,[1] L. J. Suter,[1] O. L. Landen,[1] J. P. Holder,[1] J. Schein,[1] F. D. Lee,[1] K. M. Campbell,[1] F. A. Weber,[1]

D. G. Pellinen,[2] M. B. Schneider,[1] J. R. Celeste,[1] J. W. McDonald,[1] J. M. Foster,[3] C. Niemann,[1] A. J. Mackinnon,[1]

S. H. Glenzer,[1] B. K. Young,[1] C. A. Haynam,[1] M. J. Shaw,[1] R. E. Turner,[1] D. Froula,[1] R. L. Kauffman,[1] B. R. Thomas,[3]

L. J. Atherton,[1] R. E. Bonanno,[1] S. N. Dixit,[1] D. C. Eder,[1] G. Holtmeier,[1] D. H. Kalantar,[1] A. E. Koniges,[1]

B. J. MacGowan,[1] K. R. Manes,[1] D. H. Munro,[1] J. R. Murray,[1] T. G. Parham,[1] K. Piston,[1] B. M. Van Wonterghem,[1]

R. J. Wallace,[1] P. J. Wegner,[1] P. K. Whitman,[1] B. A. Hammel,[1] and E. I. Moses[1]

[1]*LLNL, P.O. Box 808, Livermore, California 94550, USA*

[2]*Bechtel-NV, Livermore, California 94550, USA*

[3]*AWE Aldermaston, Reading, RG7 4PR, United Kingdom*

The first hohlraum experiments on the National Ignition Facility (NIF) using the initial four laser beams tested radiation temperature limits imposed by plasma filling. For a variety of hohlraum sizes and pulse lengths, the measured x-ray flux shows signatures of filling that coincide with hard x-ray emission from plasma streaming out of the hohlraum. These observations agree with hydrodynamic simulations and with an analytical model that includes hydrodynamic and coronal radiative losses. The modeling predicts radiation temperature limits with full NIF (1.8 MJ), greater, and of longer duration than required for ignition hohlraums.

The soft x-ray environment created in high-*Z* hohlraums heated by energetic laser beams, that enter the hohlraums through their laser entrance holes (LEH), is used to drive fuel capsules in indirect-drive inertial confinement fusion (ICF) experiments and to drive physics packages in high energy density (HED) studies [1]. It has been shown analytically [2] that plasma filling by hohlraum wall ablation [3,4] imposes an upper bound to hohlraum x-ray production. Current simulations indicate that hohlraums used in ICF are optimized to drive a fusion capsule to ignition before reaching the x-ray production limits. On the other hand, many HED applications [5,6] require a long sustained soft x-ray drive [7,8]. These experiments will approach the limits in T_R-τ space, where T_R is the hohlraum peak radiation temperature and τ is the time at which the internal hohlraum radiation flux will begin to drop or roll over, even before the laser pulse terminates. This occurs when the ablated hohlraum wall plasma reaches a density threshold that prevents the laser from propagating into the hohlraum due to absorption or backscattering. It was originally proposed [2] that this rollover time τ is determined by laser-plasma instabilities when the plasma density approaches $0.1n_c$, where $n_c[\mathrm{cm}^{-3}] = 1.1 \times 10^{21}/\lambda^2[\mu\mathrm{m}^2]$ is the critical density for laser light of wavelength λ. However, hohlraum experiments with short laser pulse duration have performed properly well beyond the time at which they fill to $0.1n_c$ [9,10] indicating that a critical experimental test of hohlraum fill modeling is required for assessing long radiation drive options. In this Letter we present results from experiments, numerical simulations, and analytic modeling, demonstrating vacuum hohlraum performance with a sustained radiation drive over time scales consistent with a higher fill density limit.

The National Ignition Facility (NIF) that is currently under construction [11] is a 192 laser beam system that is designed to deliver up to 1.8 MJ of energy at a wavelength of $\lambda_0 = 351$ nm. The laser is designed for indirect-drive ICF and will also be used for a variety of HED experiments. Recently, the first four laser beams were activated and experiments were performed successfully to study laser beam propagation in long scale plasmas with lengths of gas-filled ignition hohlraums [12]. In this study we present the first hohlraum experiments on the NIF that employ its unique capability to provide long, steady laser drives with variable pulse lengths, up to 20 ns. In these experiments constant power (flattop) laser pulses with 100 ps rise and fall times were used, with pulse lengths between 2 and 9 ns and energies between 5 and 17 kJ.

We used cylindrical Au hohlraums of various sizes with a single LEH and irradiated the hohlraum back wall with the four laser beams, effectively forming an $f/8$ cone that propagates along the hohlraum axis. Full aperture phase plates [13] and polarization smoothing [14] were installed on the laser beams providing a uniform intensity profile spot with a radial profile that is approximated by a $n = 5$ super-Gaussian with a 500 μm diameter ($1/e$ points) with best focus placed at the LEH [12]. The Au hohlraum walls were 5 μm thick, backed by a 100 μm CH coating, allowing us to measure spatially resolved Au *L*-shell emission (>9 keV) and to infer the hohlraum plasma fill dynamics [15]. We used a gated framing camera filtered for photon energies >6 keV with 100 μm Al; however, when viewing side-on through the 5 μm thick hohlraum Au walls the total filtering transmits >9 keV x rays.

The hohlraum radiation temperature was measured with temporal and spectral resolution through the LEH at 21.6°

with an 18-channel absolutely calibrated soft x-ray power diagnostic, Dante [16]. Dante has a partial view of the initial laser spots on the hohlraum back wall and provides a measure of the radiation flux that includes both the primary laser-plasma emission and the reemitting walls [see Fig. 2(a)]. The total backscattered laser energy measured with a full aperture backscattering station (FABS) [17], and a near backscattering imager (NBI) [18] was <0.6%. A static x-ray imager (SXI) confirmed that the beams propagate through the LEH without striking the outside walls of the hohlraum. Finally, the hot electron production inside the hohlraum was inferred from 20–100 keV absolutely calibrated x-ray spectra of the electron bremsstrahlung emission [19]. The measured hot electron fraction (temperature) was $< \sim 1\%$ (30 keV) in all hohlraums except the smallest, scale-3/4 hohlraum where it was 4% (30 keV), in good agreement with previous $\lambda_0 = 351$ nm experiments [1].

A series of experiments using 2 ns flattop pulses and variable laser energy in the 5–13 kJ range was first performed to measure the radiation temperature scaling with laser power and hohlraum size in a regime similar to previous hohlraums [9,10,20–23] where minimal plasma filling is expected. Measurements were compared to 2D LASNEX radiation-hydrodynamics simulations [24,25] using the exact hohlraum geometry, measured laser power history, and a radially symmetric approximation to the combined spatial profile of the slightly diverging 4 beams. Table I shows measured and LASNEX predicted peak radiation temperatures for scale-1 (1.6 mm diameter, 1.5 mm long) and a scale-3/4 (1.2 mm diameter, 1.1 mm long) hohlraums with LEH sizes of 0.75 of the hohlraum diameter. The peak radiation temperature scales as expected with both the laser power and hohlraum size [21] and agrees with LASNEX simulations within the 2% Dante radiation temperature error bar.

In the scale-1 2 ns pulse hohlraums the 9 keV side-on emission is localized at the back wall, indicating negligible plasma filling. Figure 1(a) shows that when irradiated by a longer 6 ns laser pulse the Au L-shell emission in the LEH region for a scale-1 hohlraum (0.8 mm LEH) eventually dominates as a result of plasma filling. We apply LASNEX simulations to calculate the ablation from the gold hohlraum walls by soft x rays and the cylindrically inward motion of the ablated plasma [Fig. 1(c)]. First, the low-

TABLE I. Peak radiation temperature measured with Dante and calculated for 2 ns flattop laser pulses vs hohlraum scale and laser power.

Laser Power (TW)	Scale	Peak Dante Tr (eV)	Calculated Peak "Dante" Tr
2.5	1	188	185
4.8	1	221	218
6.6	1	240	236
6.7	0.75	276	277

density ablation plasma moves into the beams' path and is directly heated by the laser beams. This creates a high plasma pressure on the hohlraum axis retarding complete closure of the hohlraum, which is an important part of the hydrodynamics. Second, rollover of the internal radiation temperature occurs at ~4 ns when the ablated plasma moving inward from the LEH begins to significantly absorb and refract the beam at the LEH. At this time, $n_e \sim 0.25 n_c$ at the center of the LEH and $>0.5 n_c$ at the outside of the beam. By 5.6 ns the LEH plasma completely absorbs the laser beams. As a consequence, the hard x-ray radiation production migrates from the hohlraum back wall to the region of the LEH, well reproduced by LASNEX post processed calculations of the Au L-shell emission [Fig. 1(b)].

In addition to the scale-1 hohlraum irradiated with a 6 ns laser pulse, we performed long pulse experiments using larger, scale-3/2 hohlraums (2.4 mm diameter, 2.25 mm long, 1.4 mm LEH) demonstrating that our modeling correctly predicts the size scaling of plasma fill limits and the rollover of the internal radiation temperature. With the same 6 ns laser pulse into the larger scale-3/2 hohlraum, the Au L-shell emission remains considerably stronger at the back wall than at the LEH, indicating that the hohlraum fill plasma density is moderate and that the laser still propagates into the hohlraum until the end of the laser pulse.

Figure 2 shows the radiation temperature through the LEH T_{LEH} for the 6 ns pulse experiments measured by Dante, and simulated by LASNEX. Here T_{LEH} is the equivalent radiation temperature inferred from the absolute flux measured by Dante by using Flux $(W/sr) = A_{LEH} \sigma T_{LEH}^4 \cos(21.6°)/\pi$, where A_{LEH} is the LEH area and σ is the Boltzmann constant. Figure 2 also shows the corresponding measured and simulated "M-band flux"
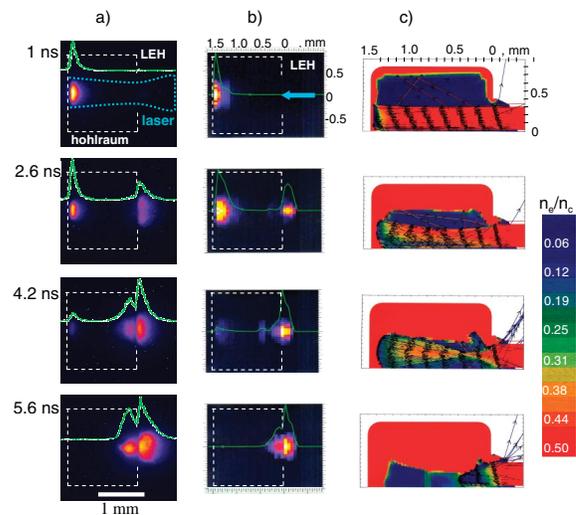
FIG. 1 (color). Side-on hard x-ray gated images and the corresponding axial intensity profiles (a) measured and (b) calculated in scale-1 hohlraum heated by 2.7 TW, 6 ns laser pulse. (c) Cross-section of electron density profiles and laser ray propagation calculated with 2D LASNEX code.
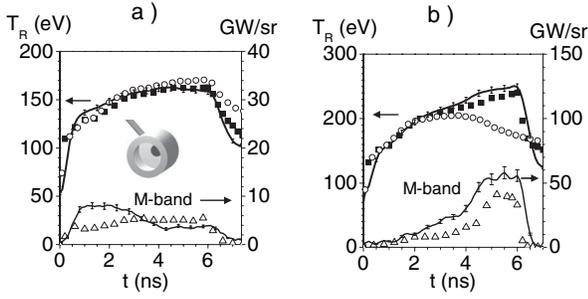
FIG. 2. Radiation temperature history as measured by Dante through LEH (thick solid line) and as simulated by LASNEX (full squares). Circles are predicted internal radiation temperatures. Measured (thin solid line) and calculated (triangles) M-band (>2 keV) flux are plotted on the right scale. (a) scale-3/2 and (b) scale-1 hohlraums driven by 2.7 TW in 6 ns flattop laser pulse. Dante view of typical hohlraum target with initial laser spots on the wall shown as dark circle shown as inset on (a).

(radiation >2 keV). The 6 ns scale-1 results [Fig. 2(b)] show two characteristic signatures of rollover not seen in the 6 ns scale-3/2 result [Fig. 2(a)]. Most prominent is the rise in Au M-band flux. These >2 keV x rays are emitted by the hot LEH plasma that absorbs the laser beams and for which Dante has a direct line of sight. In order to infer a rollover time τ from our experiments, we use the time of the sudden rise in Au M-band flux. A less prominent but simultaneous signature of the rollover is a sudden rise in the spectrally integrated T_{LEH}. Further, Fig. 2 shows the calculated "internal T_R," which is the radiation temperature that would drive an HED package located inside the hohlraum. This calculation shows "rollover" at the time τ [Fig. 2(b)] when the LEH plasma is dense enough to absorb entirely the laser energy that coincides with the sudden rise in M-band emission and the rise in LEH temperature.

In addition to detailed numerical simulations, these results can be understood and extrapolated to higher laser energies by applying a simple analytic model for radiation temperature limits. This model is based on the increased hydrodynamic losses and thin coronal radiative losses proportional to n_e^2 (n_e-electron density) [20] that occur when the laser absorption region migrates to the LEH as the hohlraum fills with plasma, leading to the rollover in the internal radiation temperature. In our model these losses become important at the LEH when the inverse bremsstrahlung absorption length λ_{IB} [26] in the laser heated plasma becomes shorter than the LEH radius r:

$$\lambda_{\mathrm{IB}} = T_e^{1.5}/200Z_H n_e^2 = 0.7r \quad (1)$$

where λ_{IB} and r are in units of cm, Coulomb logarithm is set to 7, n_e is the electron density in units of critical density n_c for the laser wavelength used, T_e is the electron temperature in keV, and Z_h is the average coronal charge state of the plasma fill. Equating the inverse bremsstrahlung absorption to the electron conduction losses away from the laser heated channel inside the hohlraum sets one constraint on n_e and T_e [1]:

$$P_L = 0.14T_e^5/Z_h^2 n_e^2 \quad (2)$$

where P_L is the power of the flattop laser pulse in TW. The electron conduction losses are calculated according to the Spitzer model described in detail in Ref. [1] approximating the laser heated channel as spherical. Pressure balance between the laser heated plasma fill and the cold x-ray ablated Au wall with average ion density n_i and charge state Z defines another constraint on n_e and T_e [1]:

$$10n_e T_e = Zn_i T_R \quad (3)$$

where the factor of 10 accounts for the internal radiation temperature T_R that is expressed in units of heV, and n_i is in units of critical density. The average x-ray ablated ion density is proportional to the ablated wall areal mass density divided by the hohlraum radius R. For a Au cylindrical hohlraum wall [1] this gives us a relation between the ion density n_i and T_R:

$$n_i = 0.0007T_R^{1.86}t^{0.54}/R \quad (4)$$

where the hohlraum radius R is in cm and t is the time after the start of the laser drive. The average x-ray ablated Au ionization state Z as a function of the radiation temperature T_R is given by $Z = 23T_R^{0.45}$ [1] and the average laser heated Au ionization state Z_H as a function of electron temperature T_e is given by $Z_H = 45T_e^{0.2}$ [27].

Another relation between the internal radiation temperature T_R, t, and R is given by a traditional hohlraum power balance omitting thermal radiation losses out of the LEH which are lower than wall losses for the LEH sizes used here. This power balance assuming constant x-ray conversion efficiency (C.E.) of 75% and 100% absorbed laser energy is given by [1]

$$P_L \propto T_R^4 R^2(1-\alpha) = 110T_R^{3.3}R^2/t^{0.4} \quad (5)$$

where the radiative wall loss fraction is $(1-\alpha) = 0.45/T_R^{0.7}t^{0.4}$. This assumes a cylindrical halfraum with length $L = 2R$, as in the experiments described here. Combining Eqs. (1)–(5) gives the rollover radiation temperature $T_{\mathrm{max}} = T_R(\tau)$ in terms of laser power, rollover time τ and LEH radius r:

$$T_{\mathrm{max}} = 1.0P_L^{0.20}/r^{0.20}\tau^{0.07} = 1.0E_L^{0.20}/r^{0.20}\tau^{0.27} \quad (6)$$

where T_{max} is in heV units, the flattop laser power (energy) P_L (E_L) is in TW (kJ), the rollover time τ is in ns, and the LEH radius r is in cm. The middle expression in Eq. (6) is applicable when the laser is power limited and the (right-hand) expression is applicable when the pulse length is long enough that the laser is energy limited. The relations (1)–(5) can be used to derive all significant hohlraum plasma parameters.

Figure 2(b) shows that the simulated Dante (T_{LEH}) and internal (T_R) temperatures have similar values at the rollover time. Hence, on Fig. 3, we can compare the experimental Dante T_{LEH} at the rollover time to T_{max} [Eq. (6)], showing good agreement. Included are data points for the
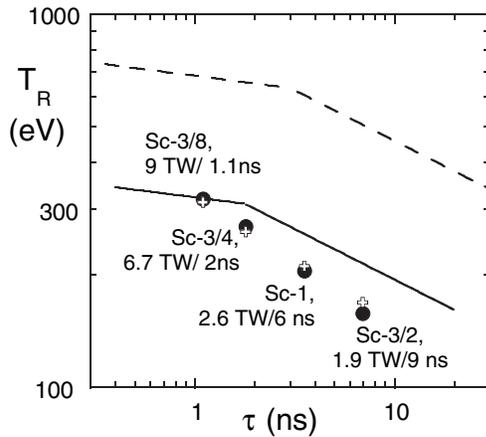
FIG. 3. Dante measured temperatures T_{LEH} at the rollover time τ and the corresponding analytical limits (crosses) calculated with Eq. (6) using experimental values of LEH radius r and laser power. Continuous and dashed black lines are Eq. (6) analytic model limits for a constant LEH radius $r = 0.3$ mm for 9 TW, 16 kJ 1 quad NIF halfraums and for 600 TW, 1.8 MJ NIF hohlraum.

scale 3/4 (Table I) which showed significant LEH emission at the end of the pulse and for a smaller scale-3/8 hohlraum, heated by a 1.1 ns laser pulse [28]. By contrast, we calculate, as expected, that the T_{max} limits per Eq. (6) are significantly higher than the measured temperatures for the 2 ns short duration, scale-1 hohlraums exhibiting negligible plasma filling (see Table I, scale 1). Figure 3 also shows analytical curves that describe the T_R limits [Eq. (6)] imposed by plasma filling for both the current NIF first quad experiment and for future experiments with the full NIF laser facility used to heat hohlraums with 192 beams through two LEHs. The two curves are calculated using Eq. (6) assuming a minimum LEH radius of 0.3 mm, dictated by the minimum NIF laser spot size and a maximum angle of incidence of 50°, and in the case of the full NIF hohlraum, an aspect ratio of $L = 3R$. Extrapolating our analytic model predictions to full NIF hohlraum performance limits suggests a maximum achievable radiation temperature of $T_{max} > 700$ eV.

In conclusion, we have demonstrated hohlraum performance limits consistent with simulations and analytic modeling for both low and high plasma filling conditions. The onset of significant plasma filling inferred by gated images of Au L-shell emission and the time dependence of the softer Au M-band flux measured by Dante were used to determine the rollover time τ. The agreement between measurements and detailed LASNEX calculations constitute compelling evidence that the dynamics of bulk hohlraum filling is well understood. Furthermore, these observations agree with our analytical model that allows us to predict the radiation production limits for full NIF in $T_R - \tau$ space. In our model the rollover of the internal T_R occurs when hydrodynamic and coronal radiative losses out of the

LEH become the dominant power loss contributors. The model can be easily extrapolated to other hohlraum geometries by modifying the constant in Eq. (4). For example, a spherical hohlraum [29] of equivalent surface area and LEH radius offers a larger volume (longer fill time), and hence T_{max} is about 5% higher. These are the first results that corroborate the limits imposed by hohlraum plasma filling in hohlraum radiation performance for indirect-drive ICF and HED experiments.

[1] J. D. Lindl, Phys. Plasmas **2**, 3933 (1995); J. D. Lindl *et al.*, Phys. Plasmas **11**, 339 (2004).
[2] B. Thomas, AWE (private communication).
[3] G. D. Tsakiris and R. Sigel, Phys. Rev. A **38**, 5769 (1988).
[4] R. M. Stevenson *et al.*, Phys. Rev. Lett. **94**, 055006 (2005).
[5] J. Massen *et al.*, Phys. Rev. E **50**, 5130 (1994).
[6] A. Benuzzi *et al.*, Phys. Rev. E **54**, 2162 (1996).
[7] B. Remington *et al.*, Metall. Mater. Trans. A **35A**, 2587 (2004).
[8] C. A. Back *et al.*, Phys. Rev. Lett. **84**, 274 (2000).
[9] S. H. Glenzer *et al.*, Phys. Rev. Lett. **80**, 2845 (1998).
[10] E. Dattolo *et al.*, Phys. Plasmas **8**, 260 (2001).
[11] G. H. Miller, E. I. Moses, and C. R. Wuest, Nucl. Fusion **44**, S228 (2004).
[12] S. H. Glenzer *et al.*, Nucl. Fusion **44**, S185 (2004).
[13] J. A. Menapace, S. N. Dixit, F. Y. Genin, and W. F. Brocious, SPIE Int. Soc. Opt. Eng. **5273**, 220 (2004).
[14] D. H. Munro, S. N. Dixit, A. B. Langdon, and J. R. Murray, Appl. Opt. **43**, 6639 (2004).
[15] L. J. Suter *et al.*, Rev. Sci. Instrum. **68**, 838 (1997).
[16] E. L. Dewald *et al.*, Rev. Sci. Instrum. **75**, 3759 (2004).
[17] D. Froula *et al.*, Rev. Sci. Instrum. **75**, 4168 (2004).
[18] A. J. Mackinnon *et al.*, Rev. Sci. Instrum. **75**, 4183 (2004).
[19] J. W. McDonald *et al.*, Rev. Sci. Instrum. **75**, 3753 (2004).
[20] L. J. Suter *et al.*, Phys. Plasmas **3**, 2057 (1996).
[21] R. Sigel *et al.*, Phys. Rev. Lett. **65**, 587 (1990).
[22] J. Massen, G. D. Tsakiris, and R. Sigel, Phys. Rev. E **48**, 2073 (1993).
[23] K. Eidmann *et al.*, Phys. Rev. E **52**, 6703 (1995).
[24] G. B. Zimmerman and W. L. Kruer, Comments Plasma Phys. Control. Fusion **2**, 51 (1975).
[25] L. J. Suter *et al.*, Phys. Rev. Lett. **73**, 2328 (1994).
[26] T. W. Johnston and J. M. Dawson, Phys. Fluids **16**, 722 (1973).
[27] R. W. Lee *et al.*, J. Quant. Spectrosc. Radiat. Transfer **58**, 737 (1997).
[28] D. Hinkel *et al.*, Phys. Plasmas **12**, 056305 (2005).
[29] J. M. Wallace *et al.*, Phys. Rev. Lett. **82**, 3807 (1999).